# Structural, Impedance, Dielectric and Modulus Analysis of $Li_{0.5-x}La_{0.5}Ti_{1-x}Nb_xO_3$ ($x = 0$, 0.05, 0.1, and 0.15)

K. Vijaya Babu*, V. Veeraiah and P.S.V. Subba Rao

Department of Physics, Andhra University, Visakhapatnam-530 003, India

*(Received November 7, 2011; revised version April 9, 2012; in final form June 19, 2012)*

The perovskite lithium lanthanum titanate shows high ionic conductivity at room temperature. Doping the lithium lanthanum titanate by niobium preserves the perovskite structure, which is synthesized by ceramic technology at high temperature (1300 °C). The X-ray diffraction and scanning electron microscopy results show that the samples exhibit single phase. AC impedance measurements indicate total conductivity of about $8.93 \times 10^{-4}$ S/cm for composition of $x = 0.05$ at room temperature. The Raman spectra and cyclic voltammetry results of the compound are also reported.

PACS: 61.05.cp, 68.37.Hk, 78.30.−j, 66.10.Ed

## 1. Introduction

In recent years, much attention has been paid to materials with perovskite and perovskite-like materials, with general formula $ABO_3$ which are of particular interest as ionic conductors [1, 2]. The ideal perovskite has a cubic unit cell of side length about 3.9 Å, the space group $Pm3m$ and $Z = 1$. The great interest in the investigation of lithium-ion conductors is intended by their considerable potential for use as solid electrolytes. These applications are offered by $Li_{0.5}La_{0.5}TiO_3$ perovskite, which possess high conductivity $1 \times 10^{-3}$ S/cm at room temperature [3, 4]. The conductivity of these compounds depends on the relationship between the concentrations of lithium ions and A-site vacancies and also effect of Ti site substitutions on the ionic conductivity of the materials.

In the present paper we discuss the system $Li_{0.5-x}La_{0.5}Ti_{1-x}Nb_xO_3$ ($x = 0$, 0.05, 0.1, and 0.15) which is based on $Li_{0.5}La_{0.5}TiO_3$ with substitution of Nb. Special attention is given to phase formation, crystal structure, impedance, and modulus analysis of the oxides.

## 2. Experimental

### 2.1. Preparation

The $Li_{0.5-x}La_{0.5}Ti_{1-x}Nb_xO_3$ ($x = 0$, 0.05, 0.1, and 0.15) (LLTN) materials are prepared by solid state reaction method

$$(0.25 - x/2)Li_2O + 0.25La_2O_3 + (1-x)TiO_2 + (x/2)Nb_2O_5 \rightarrow Li_{0.5-x}La_{0.5}Ti_{1-x}Nb_xO_3$$
$$(x = 0,\ 0.05,\ 0.1,\ \text{and}\ 0.15).$$

The starting materials are lithium oxide (Merck 99.9%), lanthanum(III) oxide (Himedia 99.9%), titanium(IV) oxide (Sigma–Aldrich 99%) and niobium(V) oxide (Himedia 99.9%) which are mixed in stoichiometric ratio. Raw chemicals with high purity are used for the material preparation. The constituents of required specimen are taken in a stoichiometric ratio and dry mixed followed by wet mixing with methanol as medium. The mixing is accomplished using agate mortar and pestle. The powder is calcined at 500 °C for 4 h and at 800 °C for 4 h and then cooled to room temperature. The calcined powder was ground and calcined again at 1150 °C for 12 h. After calcination, the powder is ground again and is mixed with polyvinyl alcohol (PVA) (which acts as binder) to reduce the brittleness and to have better compactness among the granules of the material. The pellets of dimension 10 mm diameter and 1 or 2 mm thickness are made using hydraulic (KEROY) press with the help of stainless steel dye. The pellets are sintered at 1300 °C for 6 h using platinum foil to increase the density.

### 2.2. Experimental techniques

The phase constitutes of the calcined sample were identified by X-ray diffraction with RIGAKU X-ray diffractometer Ultima III (with Cu $K_\alpha$ radiation, $\lambda = 1.5402$). The microstructure of the sintered samples was characterized by scanning electron microscopy (SEM) (Carl Zeiss, EVO MA 15, Oxford Instruments, Inca Penta FET x3.JPG). Raman experiments were carried out for the calcined sample (Nicolet 6700 FT-Raman spectrometer). The spectra were recorded from 0 to 1000 $cm^{-1}$. The conductivity for the sample was measured by an AC impedance technique. The bulk resistances of the composite electrolyte systems are computed from the complex impedance plots with the help of LCR Bridge (HIOKI, model 3532-50, Japan) operating in the frequency range of 42 Hz to 5 MHz and the temperature range from 30 °C to 150 °C. The cyclic voltammograms are recorded within the potential range −2.0 to 3.0 V at the scanning rate of 0.05 mV/s at room temperature using the Electrochemical workstation, CH instrument (CHI 760C).

* corresponding author; e-mail: vijayababu.k@gmail.com

## 3. Results and discussion

### *3.1. X-ray diffraction*

The X-ray diffraction patterns of calcined $Li_{0.5-x}La_{0.5}Ti_{1-x}Nb_xO_3$ ($x = 0$, 0.05, 0.1, and 0.15), in which the Bragg reflections have been indexed as a cubic unit cell $Pm3m$ ($Z = 1$), are shown in Fig. 1. The $Nb^{5+}$ ions occupy the octahedral interstitial and $La^{3+}$ ions locate at the corner of the cubic unit cell. Recently, the attention has been paid again to the niobium doping into the B sublattice, where $Nb^{5+}$ substitutes $Ti^{4+}$, bringing more oxide ions or more electrons into the system [6, 7]. Due to the electrostatic interaction among the constituent ions, the ordering of the A-site vacancies along the $c$-axis occurs naturally. Simultaneously, $Nb^{5+}$ ions are reduced to $Nb^{4+}$. The materials possessing the above properties could be used as electrode materials for the lithium-ion battery. Some impurity phases are observed in the samples with the composition of $x$ larger than $x = 0.1$. The perovskite phase was observed in the composition range from $x = 0$ to $x = 0.1$, while a small amount of $LiNbO_3$ phase with perovskite-like structure was observed in the sample at $x = 0.15$ [8, 9].

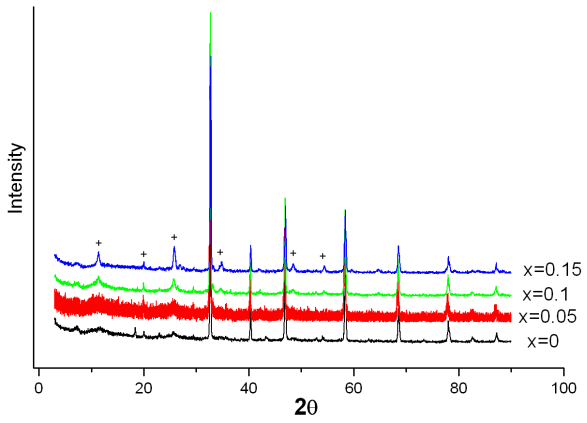


Fig. 1. XRD pattern of $Li_{0.5-x}La_{0.5}Ti_{1-x}Nb_xO_3$ ($x = 0$, 0.05, 0.1, and 0.15).

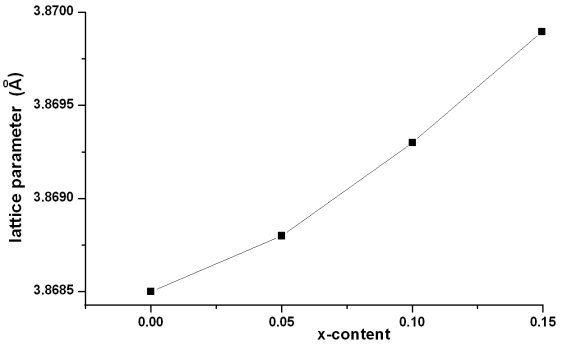


Fig. 2. Variation of lattice parameter in $Li_{0.5-x}La_{0.5}Ti_{1-x}Nb_xO_3$ ($x = 0$, 0.05, 0.1, and 0.15).

The lattice parameter and the unit cell volume of the LLTN increase with the $x$ value (Fig. 2). This is expected, as the ionic radius of the $Nb^{5+}$ (0.69 Å) is higher than that of $Ti^{4+}$.

The crystallite size was calculated by using Scherrer's formula and it is found to decrease with $x$ value. The crystallite sizes are 68.51, 62.31, 49.54, and 42.96 nm for the samples with $x = 0$, 0.05, 0.1, and 0.15, respectively.

### *3.2. Scanning electron microscopy*

Figure 3 shows the SEM micrographs for the samples sintered at 1300 °C for 6 h with $x = 0$, 0.05, 0.1, and 0.15, respectively. All sintered samples exhibit dense microstructures. The grain sizes of the samples are calculated by linear intercept method. The average grain size is calculated to be 2.2, 1.86, 1.76, and 1.71 $\mu$m for $x = 0$, 0.05, 0.1, and 0.15, respectively [10].

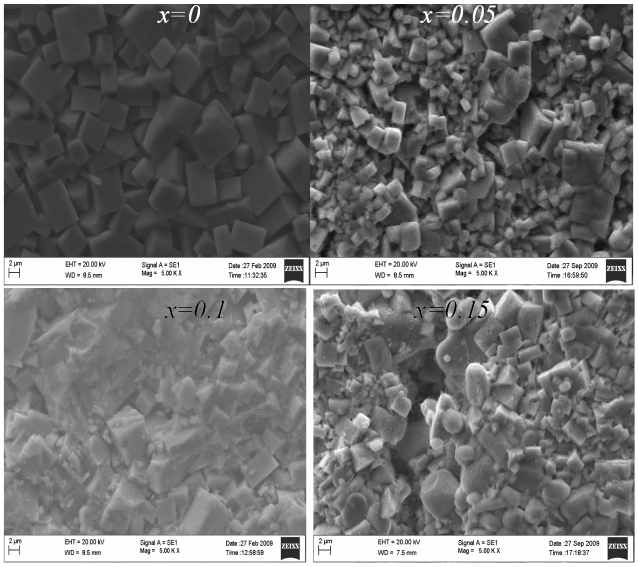


Fig. 3. SEM images of LLTN ($x = 0$, 0.05, 0.1, and 0.15).

### *3.3. Raman spectrum*

In Fig. 4 Raman spectra of LLTN ($x = 0$, 0.05, 0.1, and 0.15) are recorded at room temperature. The Raman scattering spectra are carried out using exciting laser with the wavelength $\lambda = 1.06$ $\mu$m. The spectra are obtained for calcined powder samples. The wavelengths of the peaks in particular, overlapping ones are determined by experimental data. It is possible to follow changes in positions of the peaks with concentration of the $Nb^{5+}$ dopant. There are only five apparent resonance bands in the best resolved spectra of all the samples, although from theoretical considerations one anticipates fifteen degrees of freedom per unit cell. In cubic phase it has $O_h$ symmetry and the 15 degrees of freedom divided into optical representations $3F_{1u} + F_{2u}$, while another $F_{1u}$ symmetry mode corresponds to acoustical branch [11]. The 144, 240, and 536 $cm^{-1}$ modes are arising from the $F_{1u}$ cubic phase modes. The 455 $cm^{-1}$ mode comes from

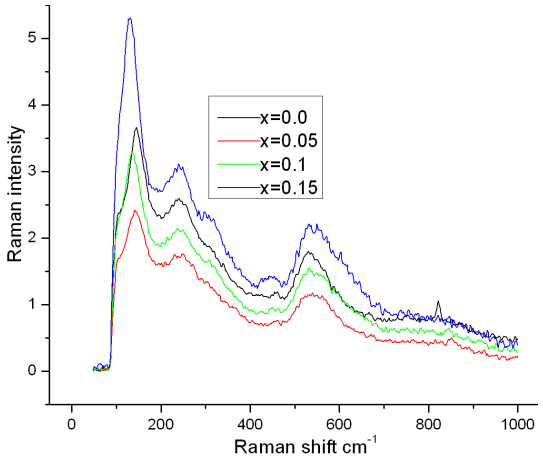


Fig. 4. Raman spectra of LLTN ($x$ = 0, 0.05, 0.1, and 0.15).

the splitting of the cubic $F_{2u}$ mode and the somewhat broader 821 cm$^{-1}$ mode is observed also as $F_{1u}$ mode.

### 3.4. Dielectric constant

The variation of dielectric constant measured at 5 MHz frequency as a function of $x$ value for LLTN ($x = 0$, 0.05, 0.1, and 0.15) is shown in Fig. 5. The dielectric constant decreases slightly with the increase in $x$ value. According to the Clausius–Mossotti (C–M) equation, the dielectric constant increases with increasing total dielectric polarizability $\alpha_D$ and decreasing unit cell volume. The unit cell volume was estimated from XRD data and changed little from 57.8932 (Å)$^3$ for $x = 0.0$ sample to 58.1045 (Å)$^3$ for $x = 0.15$ sample. The effect of $\boldsymbol{\alpha}_D$ on dielectric constant is much larger than that of unit cell volume [12]. A small change of $\boldsymbol{\alpha}_D$ will result in large variation of dielectric constant. So the dielectric constant should be decreased with increasing lithium content, which is in agreement with the results in Fig. 5. The dielectric constant of the sample is much lower at $x = 0.15$.

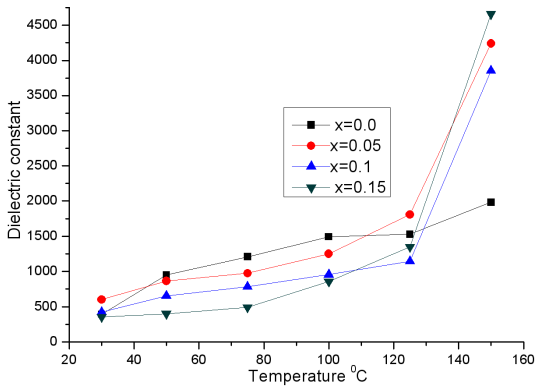


Fig. 5. Variation dielectric constant as a function of $x$ value for LLTN ($x = 0$, 0.05, 0.1, and 0.15).

### 3.5. Impedance analysis

Figure 6 shows the Cole–Cole plots of $Li_{0.5-x}La_{0.5}Ti_{1-x}Nb_xO_3$ obtained from impedance

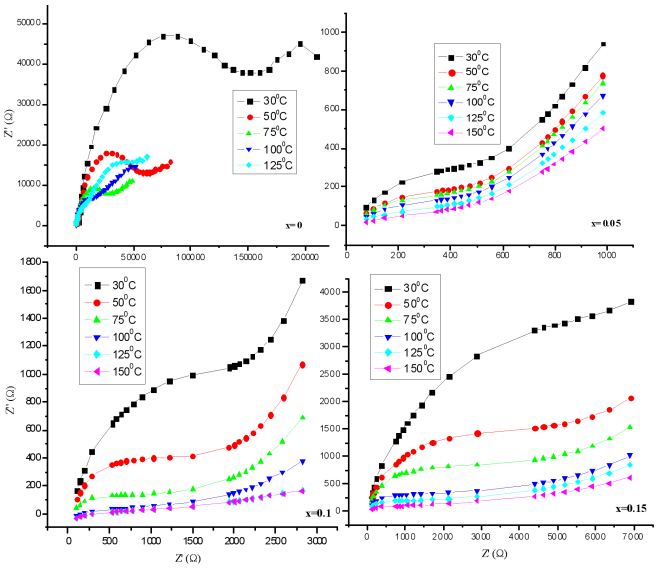


Fig. 6. Cole–Cole plot LLTN ($x$ = 0, 0.05, 0.1, and 0.15).

measurements. The bulk resistance of the sample is estimated from the crossing point of the extrapolated semicircle with the real axis at lower frequency range. The conductivity can be expressed as $\sigma = \omega\varepsilon_0\varepsilon''$, where $\varepsilon_0$ is the dielectric permittivity in air; $\omega$ is the angular frequency $= 2\pi f$ and $\varepsilon'' = \tan\delta\varepsilon'$. Since the conductivity of all the samples is estimated to be of the order of $10^{-4}$ to $10^{-5}$ S/cm at room temperature, the electric conduction of the samples might be almost ionic.

Up till now, the bulk and grain boundary conductivity values reported on LLT are subjected to large variations even for the same composition. Suppose the bulk conductivity of $Li_{1/2}La_{1/2}TiO_3$ falls in the range of $10^{-5}$–$10^{-3}$ S/cm at room temperature. This variation indicates that the sample preparation conditions such as sintering temperature may have a great influence on the ionic conductivity. We expect this since the volume fractions of grains and grain boundaries in specimen vary with the grain size, and the grain size normally varies with the sintering temperature and duration. Furthermore, the carrier concentration may also be altered due to possible evaporation of lithium during sintering. Therefore, pre-optimization of the sample preparation process, particularly the sintering process will be of utmost importance in the present case in order to rule out the possibility that any difference in conductivity is due to the difference in microstructure rather than due to the doping effect.

The conductivity of all samples increases with increase of temperature. With the decrease in the amount of $Li^+$ ions due to the substitution of $Nb^{5+}$ for $Ti^{4+}$ and $Li^+$, the

conductivity decreased with increasing $Nb^{5+}$ fraction $x$, while the activation energy for ionic conduction increased with increasing $x$ value [13]. Allowing the fraction of vacancy in A-site being always constant, this indicates that the mobility of $Li^+$ ions would increase accompanying the increase of conductivity because of the expansion of the lattice by the substitution of $Nb^{5+}$ for $Li^+$ and $La^{3+}$.

The highest value of the conductivity ($8.93 \times 10^{-4}$ S/cm) is obtained for the material with composition corresponding to $x = 0.05$ and the conductivity decreases with increasing the content [14]. The lithium lanthanum niobium titanate at $x = 0.05$ presents a higher conductivity than the corresponding lithium lanthanum titanate. The conductivity is also higher than the titanates of other rare earths.

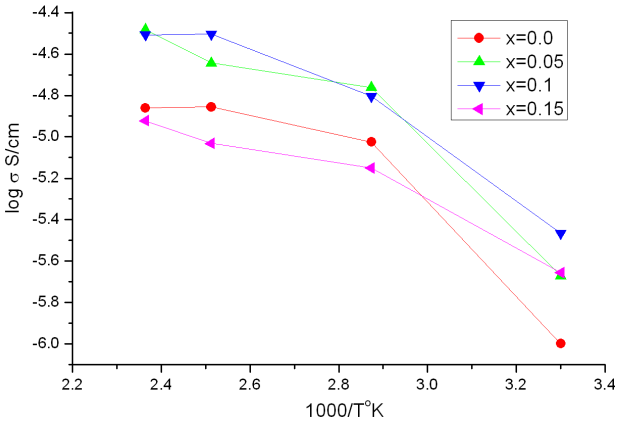


Fig. 7. Arrhenius plots (AC) for different compositions.

The activation energy (0.257 eV) increases gradually up to $x = 0.15$ (Fig. 7). The activation energies indicate that the differences in conductivity come from differences in the pre-exponential factors.

### *3.6. Modulus analysis*

The modulus analysis has an advantage that it suppresses the information about electrode effects. This can also be used to study conductivity relaxation times. The complex modulus is defined as the inverse of the complex permittivity. In the present work, the impedance data were converted into electrical modulus by using the relation $M' = \omega C_0 Z'$ (real part) and $M'' = \omega C_0 Z''$ (imaginary part), where $C_0 = \varepsilon_0 A/L$, $A$ is the area of the sample, L is the thickness of the sample and $\varepsilon_0$ is the permittivity of the free space ($8.854 \times 10^{-14}$ F/cm) [15].

The macroscopic behavior of a dielectric can be understood by considering the dielectric in between a parallel plate capacitor. The capacitance ($C$) of the capacitor with the dielectric is

$$C = \varepsilon_r \varepsilon_0 A/d,$$

where $\varepsilon_r = \varepsilon/\varepsilon_0$ is the dielectric constant of the dielectric. It is also called as relative permittivity, $\varepsilon$ is called the permittivity of the dielectric, $\varepsilon_0$ ($8.854 \times 10^{-14}$ F/cm) is the permittivity of the free space, $A$ and $d$ are corresponding area and thickness of the plates, respectively [16]. The frequency dependence of $M'$ and $M''$ for the compound are shown in Fig. 8.

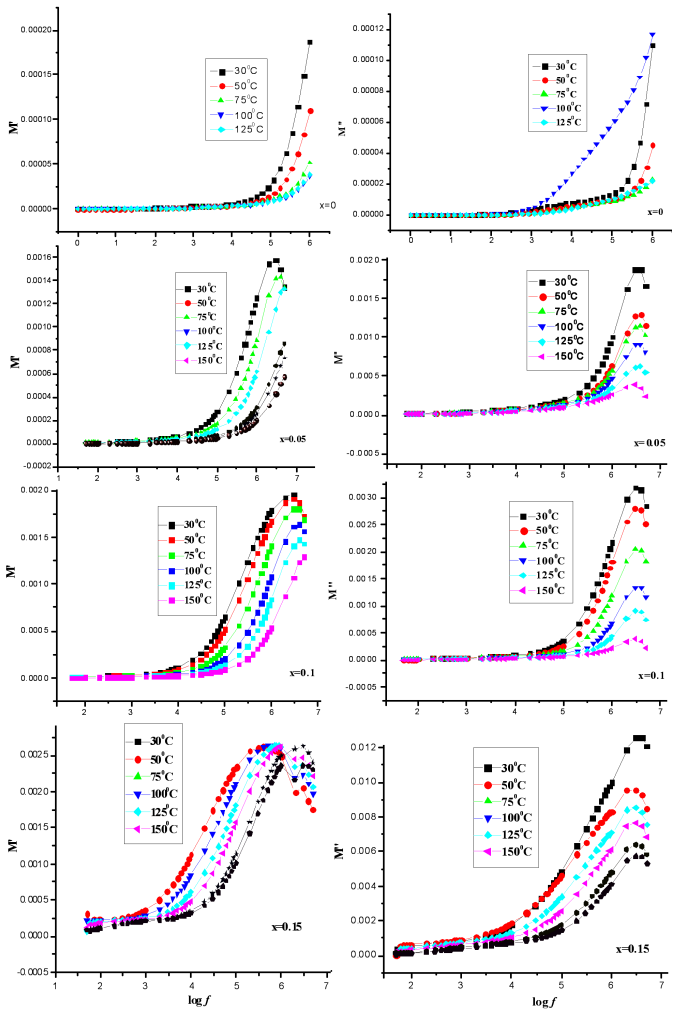


Fig. 8. Frequency dependence of $M'$ and $M''$ for LLTN ($x = 0$, 0.05, 0.1, and 0.15).

At lower frequencies, $M'$ tends to be very small, confirming that the contribution from the electrode effect is negligible. The observed dispersion in $M'$ at higher frequencies may be due to conductivity relaxation. The variation of imaginary part of electrical modulus ($M''$) of the compounds with frequency at different temperatures is shown in Fig. 8. It is observed that $M''$ decreases with increase in frequency at lower temperatures but above 100 °C, variation of $M''$ with frequency attains a maximum value (peak) at a particular frequency, and that peak is shifted to higher frequency with rise in temperature. The peak in the $M''$ vs. frequency plot is asymmetric in nature indicating the spread of relaxation time. The asymmetric nature of the modulus peak indicates the stretched exponential character of relaxation time [17].

### 3.7. Cyclic voltammetry

The cyclic voltammogram curves (Fig. 9) indicate that the electrochemical reaction is completely reversible. As

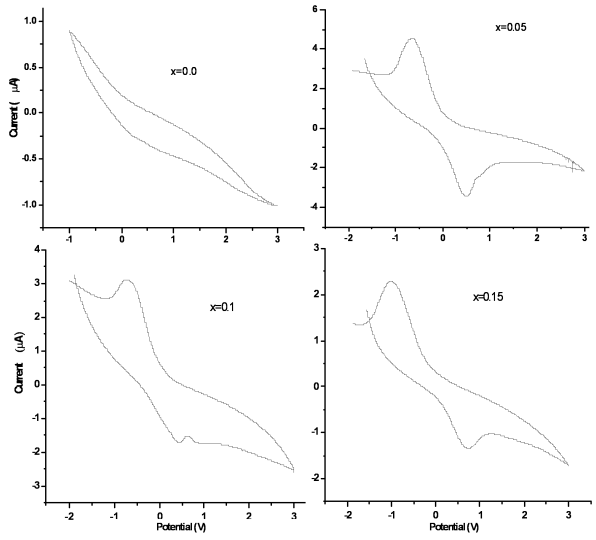


Fig. 9. Cyclic voltammograms of LLTN ($x = 0$, 0.05, 0.1, and 0.15).

the result of this reaction, electronic conductivity appears in the niobium compounds. The overall stability of the electrolytes is good with no electrochemical oxidation occurring at potentials smaller than 3 V. Therefore these materials can be used as solid electrolytes in secondary barriers down to low potential [18].

## 4. Conclusions

The lithium lanthanum niobium titanate LLTN ($x = 0$, 0.05, 0.1, and 0.15) solid electrolytes are prepared by a solid state reaction method. By X-ray diffraction analysis of the prepared samples, it is found that its crystal structure is exactly the same as the cubic perovskite. The microstructure of all samples is measured by scanning electron microscopy and the grain size is about 2 $\mu$m for all samples. The bonding nature of the samples is identified using the Raman spectroscopic studies. The impedance of LLTN ($x = 0$, 0.05, 0.1, and 0.15) electrolyte is measured in the temperature range of 30 °C to 150 °C and in the frequency range 42 Hz to 5 MHz. The activation energies for the lithium ionic conduction are estimated to be 0.2 eV. The maximum conductivity is found as $8.66 \times 10^{-4}$ S/cm at $x = 0.05$ which must be a good ionic conductor at low temperatures and a good candidate as an electrolyte for low temperature electrochemical cells. The cyclic voltammogram curves indicate that the electrochemical reaction is completely reversible.

## References

[1] S. Stramare, W. Weppener, *Ionics* **5**, 405 (1999).
[2] H.Y. Liu, W.J. Wang, S.T. Wu, *Ionics* **278**, 8 (2002).
[3] A.G. Belous, *J. Eur. Ceram. Soc.* **21**, 1797 (2001).
[4] E.A. Fortalnova, O.N. Gavrilenkov, A.G. Belous, E.D. Politova, *Russ. J. Gen. Chem.* **79**, 1987 (2009).
[5] H.T. Chung, J.G. Kim, H.G. Kim, *Solid State Ionics* **107**, 153 (1998).
[6] J. Karczewski, B. Riegel, M. Gazda, P. Jasinski, B. Kusz, *J. Electroceram.* **24**, 326 (2010).
[7] S. Hashimoto, F.W. Poulsen, M. Mogensen, *J. Alloys Comp.* **439**, 232 (2007).
[8] M. Nakayama, H. Ikuta, Y. Uchimoto, M. Wakihara, *J. Mater. Chem.* **12**, 1500 (2002).
[9] Y. Kawakami, H. Ikuta, M. Wakihara, *J. Solid State Electrochem.* **2**, 206 (1998).
[10] Ke Ye, Mi Lin Zhang, Ye Chen, Wei Han, Yong De Yan, Shu Quan Wei, Li Jun Chen, *J. Appl. Electrochem.* **40**, 1387 (2010).
[11] B. Mihailova, U. Bismayer, B. Guttler, M. Gospodinov, L. Konstantinov, *J. Phys. Condens. Matter* **14**, 1091 (2002).
[12] A.M. Varaprasad, A.L. Shashi Mohan, D.K. Chakrabarty, A.B. Biswas, *Bull. Mater. Sci.* **2**, 239 (1980).
[13] Y. Inaguma, L. Chen, M. Itoh, T. Nakamura, T. Uchida, H. Ikuta, M. Wakihara, *Solid State Commun.* **86**, 689 (1993).
[14] Y. Inaguma, L. Chen, M. Itoh, T. Nakamura, *Solid State Ionics* **70-71**, 196 (1995).
[15] N. Dridi, A. Boukhari, J.M. Reau, E. Arbib, E.M. Holt, *Solid State Ionics* **127**, 141 (2000).
[16] R. Suresh Kumar, K. Hariharan, *Mater. Chem. Phys.* **60**, 28 (1999).
[17] Jianjun Liu, Chun Gang Duan, Wei Guo Yin, W.N. Mei, R.W. Smith, J.R. Hardy, *J. Chem. Phys.* **119**, 2812 (2003).
[18] S. Garcia Martin, J.M. Rojo, H. Tsukamoto, E. Moran, M.A. Alario Franco, *Solid State Ionics* **116**, 11 (1999).